

Connecting Synchrotron, Cosmic Rays, and Magnetic Fields in the Plane of the Galaxy

T. R. Jaffe^{1,2*}, A. J. Banday^{1,2,3†}, J. P. Leahy^{4‡}, S. Leach^{5,6§}, A. W. Strong^{7¶}

¹ *Université de Toulouse; UPS-OMP; IRAP; Toulouse, France*

² *CNRS; IRAP; 9 Av. colonel Roche, BP 44346, F-31028 Toulouse cedex 4, France*

³ *Max Planck Institute for Astrophysics, Karl-Schwarzschild Str. 1, D-85741 Garching, Germany*

⁴ *Jodrell Bank Centre for Astrophysics, School of Physics and Astronomy, The University of Manchester, Oxford Road, Manchester, M13 9PL, United Kingdom*

⁵ *SISSA, Astrophysics Sector, via Beirut 2-4, I-34014 Trieste, Italy.*

⁶ *INFN, Sezione di Trieste, I-34014 Trieste, Italy.*

⁷ *Max-Planck-Institut für Extraterrestrische Physik, Postfach 1312, D-85741 Garching, Germany*

ABSTRACT

We extend previous work modeling the Galactic magnetic field in the plane using synchrotron emission in total and polarised intensity. In this work, we include a more realistic treatment of the cosmic-ray electrons using the GALPROP propagation code optimized to match the existing high-energy data. This addition reduces the degeneracies in our previous analysis and when combined with an additional observed synchrotron frequency allows us to study the low-energy end of the cosmic-ray electron spectrum in a way that has not previously been done. For a pure diffusion propagation, we find a low-energy injection spectrum slightly harder than generally assumed; for $J(E) \propto E^\alpha$, we find $\alpha = -1.34 \pm 0.12$, implying a very sharp break with the spectrum above a few GeV. This then predicts a synchrotron brightness temperature spectral index, β , on the Galactic plane that is $-2.8 < \beta < -2.74$ below a few GHz and $-2.98 < \beta < -2.91$ up to 23 GHz. We find that models including cosmic-ray re-acceleration processes appear to be incompatible with the synchrotron data.

Key words: ISM: magnetic fields – ISM: cosmic rays – Galaxy: structure – polarisation – radiation mechanisms: general – radio continuum: ISM

1 INTRODUCTION

Studies of both cosmic rays and magnetic fields in the Galaxy have independently gained momentum recently from the advent of newly available data. The Fermi satellite has recently provided the most precise direct measurements to date of the cosmic ray electron (CRE) spectrum near the Earth (Ackermann et al. 2010) as well as of the γ -ray sky that provides indirect measurements of the cosmic ray distribution in the Milky Way (Abdo et al. 2009). Recently expanded catalogs of Faraday rotation measures (RMs) by Taylor et al. (2009) and Van Eck et al. (2011) (and soon GALFACTS¹) are allowing large-scale magnetic field theories to be tested and rejected by the hugely increasing

amounts of data. And last but not least, the first full-sky maps of polarised synchrotron emission in microwave frequencies provided by the Wilkinson Microwave Anisotropy Probe (*WMAP*) (and soon the Planck satellite²) are beginning to allow us to disentangle the various degeneracies that dog studies of how the cosmic rays and the magnetic fields interact in the interstellar medium (ISM).

In Jaffe et al. (2010) (hereafter Paper I), we studied the components of the Galactic magnetic field using the three complementary datasets of total synchrotron intensity, polarised synchrotron intensity, and rotation measure. In that paper, our aim was to determine the relative strengths of the magnetic field components which we define as coherent, ordered, and random. These components can be separated by examining Faraday rotation measure to fix the coherent component and synchrotron emission to explore the ordered and random components. The geometry allows us to sepa-

* E-mail: tess.jaffe@cesr.fr

† E-mail: Anthony.Banday@cesr.fr

‡ E-mail: j.p.leahy@manchester.ac.uk

§ E-mail: leach@sissa.it

¶ E-mail: aws@mpe.mpg.de

¹ <http://www.ocalgary.ca/ras/GALFACTS/>

² <http://www.esa.int/planck>

rate them using the combination of synchrotron polarised and total intensity. See Fig. 1 from Paper I.

Ideally, we would have both such datasets at the same frequency. But we are attempting to determine the magnetic field structure in the plane of the galaxy, which brings in two complications. At frequencies below a few GHz, we cannot use polarised emission as a tracer of large-scale structure because of Faraday depolarisation; the turbulent ISM effectively imposes a polarisation horizon beyond which the polarisation signal is erased (Uyaniker et al. 2003). Above frequencies of a few GHz, however, the total intensity is dominated on the Galactic plane by free-free emission and the anomalous dust-correlated emission (generally believed to be electric dipole emission from spinning dust grains). It is not currently possible, therefore, to determine the magnetic field components via comparison of polarised and total intensity at the same frequency. In Paper I, we used a frequency for total intensity that is low enough that the synchrotron dominates, and another frequency, well above the Faraday regime, for the polarised intensity.

The drawback of this approach is the assumption of a simple power law distribution of cosmic ray electrons, $J(E) \propto E^{-p}$, over all energies with an index of $p = 3$. Given that the data span the range from the low-frequency radio at 408 MHz to the microwave at 23 GHz, this assumption is likely to introduce errors into the resulting parameters inferred for the magnetic field strength. Since two synchrotron observables I and PI allow us to determine the relative strengths of the three magnetic field components defined in Paper I, with an additional low frequency total I dataset we can additionally constrain the low-energy end of the cosmic ray electron spectrum. The first aim of this paper is to see what can be confidently measured using the available data.

It is often assumed that the low-energy CRE spectrum, i.e. below ~ 4 GeV, is harder than the spectrum in the Fermi frequencies, where the CRE spectrum has been well measured between 7 GeV and 1 TeV (Ackermann et al. 2010). Estimates of the low-energy spectral index have been done with low-frequency radio surveys (e.g., Guzmán et al. 2011), but lower than 408 MHz, one must begin to worry about and model free-free absorption, which is particularly difficult in the plane. Direct local measurements near the earth of CREs at energies below a few GeV are affected by solar modulation. Therefore, it is the synchrotron emission below a very few GHz that is likely the best method for measuring this spectrum, at least as an average in the Galactic plane. We test two possible datasets for the intermediate frequency: the 1420 MHz full-sky survey of Reich (1982); Reich & Reich (1986) and the 2326 MHz southern survey of Jonas et al. (1998).

Rather than assuming that the cosmic ray spectrum follows even a simple broken power law, we use a complete cosmic ray propagation code, GALPROP³. This allows us to use physically motivated models of cosmic ray electron and positron propagation – including treatment of diffusion, synchrotron energy losses, the local interstellar radiation field, re-acceleration, secondary production, etc.; see Strong et al. (2007) – which are consistent with the Fermi

data (Strong et al. 2010). GALPROP can give us a full four-dimensional model of the Galactic cosmic ray distribution both as a function of Galactic position and of energy. We can then integrate the synchrotron emission not only over the line-of-sight but also over the cosmic ray spectrum in order to get the best possible prediction of the synchrotron emission.

As in Paper I, we use a full Markov Chain Monte Carlo (MCMC) analysis to explore the parameter space of both the Galactic magnetic field and now also the low energy cosmic ray electron injection spectrum. We have integrated the GALPROP CRE propagation code into our HAMMURABI⁴ (Waelkens et al. 2009) simulation code, now performing the full integration over the electron spectrum rather than simply assuming an electron index of $p = 3$ as in Paper I. We now obtain a result that is fully self-consistent, in the sense that the cosmic rays are propagated through a galaxy model that includes our magnetic field model (which changes the CRE spectrum through synchrotron energy losses) and then those CREs are used to determine the total observed synchrotron emission.

The result is more reliable measurement not only a of the magnetic field parameters but also of the low-energy cosmic ray spectrum than is possible with other methods. We can then compare our result to low-energy cosmic ray data from local measurements and comment on the issue of solar modulation.

2 OBSERVATIONS

The data we use are shown as green solid lines in Fig. 1 with annotations to point out interesting features:

- *Top*: from Haslam et al. (1982), the synchrotron total intensity at 408 MHz.
- *Second*: from Jonas et al. (1998), the synchrotron total intensity at 2.3 GHz.
- *Third*: from Jarosik et al. (2011), the synchrotron polarised intensity at 23 GHz from the *WMAP* seven-year analysis.
- *Bottom*: the RM data from Brown et al. (2003, 2007) averaged into roughly 6° bins.

As described in Paper I, the sky maps are smoothed to a common low resolution FWHM of 3° . The profile at zero latitude is then extracted and an additional boxcar smoothing applied to a resolution of roughly 6° .

With the exception of the second panel down, the datasets in Fig. 1 are those used in Paper I with small modifications. For example, the *WMAP* data have been updated with the seven-year results. The free-free correction for the synchrotron total intensity has also been modified, as described in § 2.3. The second profile from the top is an additional synchrotron total intensity dataset at an intermediate frequency. (It is processed identically to the Haslam et al. data; see Paper I.) It is the addition of this dataset that will allow us to explore the cosmic ray spectrum rather than to assume a simple power law over all energies.

³ <http://galprop.stanford.edu>

⁴ <http://www.mpa-garching.mpg.de/hammurabi/>

The unsurprising fact that our model from Paper I (shown in red) clearly does not fit this profile is the motivation for this work. That model is based on a simple exponential disc for the spatial distribution of CREs (which partly determines the longitude profile's shape) and a single power law for the spectral distribution (which determines the relative amounts of emission at each frequency). The failure of the model is largely due to the over-simplistic spectrum, as we now have three frequencies with which we probe the cosmic ray spectrum, and it is not expected to be a simple power law.

Tangents to possible spiral arms are indicated, and vertical lines mark interesting sight-lines (solid for positive RM, dashed for negative), also shown on Paper I Fig. 4. The dashed orange line is the estimate for the free-free contamination which has been subtracted from the total emission at 408 MHz (dotted green line); see § 2.3.

We note that other radio surveys on the plane exist (see, e.g. the Bonn Survey Sampler⁵), but the two radio bands chosen are most appropriate for our purposes. A low frequency gives a longer lever-arm for studying the CRE spectrum and also minimizes the thermal emission on the plane. At 408 MHz, the synchrotron is sampled at sufficiently low a frequency but not so low as to be affected by absorption effects on the plane. At intermediate frequencies, there are several surveys that include the galactic plane, but many do not have sensitivity to large angular scales. We have also considered the 1420 MHz survey of Reich (1982); Reich & Reich (1986). We find, however, that on the plane this survey is not consistent with the 2.3 GHz survey. Though there are issues with both surveys, we have not found a clear explanation for this discrepancy. There is a potential issue with the 2.3 GHz survey in that it is sensitive to only one polarization direction. This may over or under estimate the total intensity depending on the orientation of the polarization relative to the detector. Given the significant depolarization at this frequency (Duncan et al. 1997, for example), we expect this effect to be quite small, of order a few percent at most. Furthermore, we note that the 2.3 GHz survey is independently calibrated on a large-angular scale drift scan measurement at 2 GHz (Jonas et al. 1998). We therefore consider the 2.3 GHz survey a better choice for this analysis on the galactic plane.

Since Paper I, new RM data have been published by Van Eck et al. (2011). These data cover part of the missing region of the plane most of interest to attempts to model the coherent field structure. The purpose of this paper, however, is simply to modify our previous analysis using more realistic CRE spectral models and an additional synchrotron total intensity frequency. To modify the coherent field model to match the van Eck et al. data is therefore beyond the current scope, though clearly we plan to incorporate the data in future work. It is interesting to note that our proposed best-fitting spiral model does not fit the new data, which we discuss more in the context of our results in § 4. But this inconsistency is only in the positions of the arms, not in the strength of the magnetic field components. It therefore does not have an impact on the current aim to constrain the CRE spectrum using the synchrotron spectrum.

⁵ <http://www.mpifr-bonn.mpg.de/survey.html>

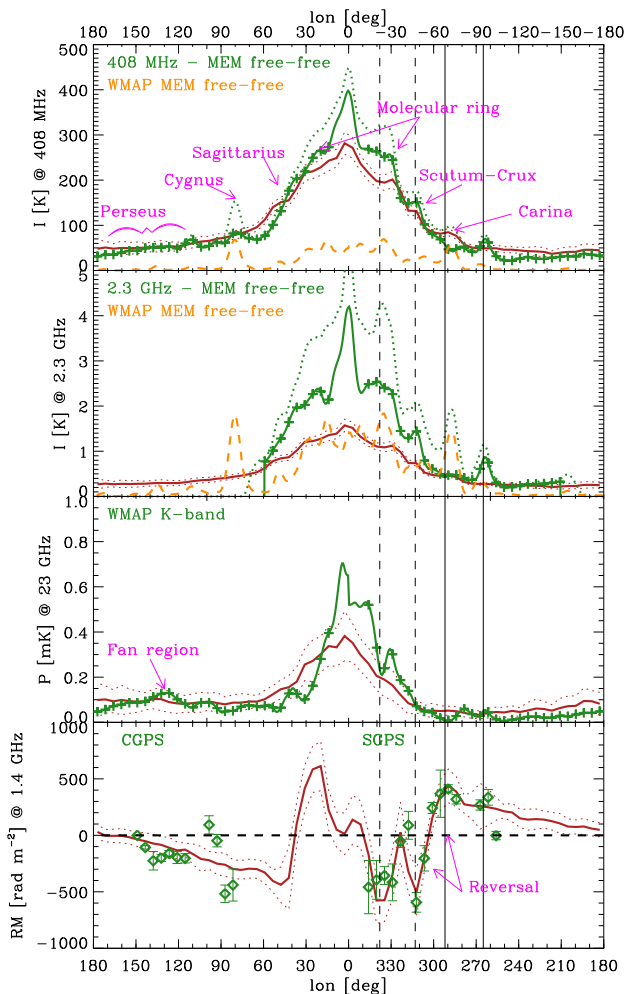


Figure 1. The available observables (green) tracing the Galactic magnetic field. The over-plotted model (red) is the original model from Paper I, while the data have been updated somewhat. See text in § 2. Furthermore, we have added the 2.3 GHz frequency which clearly shows that the power-law CRE spectrum does not match all of the data. (The dotted green line is the raw data, while the solid is that after a free-free estimate, shown in dashed orange, is subtracted. See § 2.3.)

2.1 Offsets

In Paper I, we treated all maps identically and fit an offset using a $\csc(|b|)$ model to the sky outside of the plane and subtracting that offset. At 408 MHz, this gives a surprisingly high offset, which though not particularly significant for the analysis we did is certainly much higher than the offset of 5.89 K (Lawson et al. 1987) or the offset found by Reich & Reich (1988) of 2.7 K (based on comparison to their 1420 survey).

Clearly, the synchrotron sky is not well represented by a cosecant law, as the matter distribution is not well approximated by a simple slab model. (Furthermore, depending on how it's done, it often leaves unphysical negative pixels.) Despite its shortcomings, Bennett et al. (2003) use this method as well and find that the Lawson et al. offset of 5.89 K is

sufficient and that their cosecant fits show no evidence of an additional offset. Though there are a variety of other determinations of this survey’s offset, for this work, we have decided to use the corrections given by Lawson et al. (1987) for the 408 MHz survey, i.e. we subtract an offset of 5.89 K. Note that at this frequency, the offset uncertainty is only of order 1% of the signal in the plane, and had we chosen the Reich & Reich (1988) offset, our scientific results would be effectively unchanged. We apply no additional offset correction to the 2.3 GHz survey, as the temperature scale of the survey data has been set by comparison to an absolutely calibrated survey at 2 GHz and had a prediction for extragalactic contributions removed; see Jonas et al. (1998) for details.

When also examining the free-free subtraction in the next section, we fit 408 MHz as a template to the 2.3 GHz synchrotron profile with a linear fit that essentially gives us a template scale factor based on the structure and a measure of the implied offset between the surveys, similarly to a TT-plot. As shown in Fig. 5, the fitted offset is very small and well within the quoted uncertainties.

Note that the free-free model (see 2.3) has also been examined for an offset using cosecant fits. That analysis gives offsets too small to be of significance: of order 0.07 mK at 33 GHz, which is too small to be seen in a plot such as Fig. 1 and is much smaller than any of the other uncertainties.

2.2 Processing

The LAMBDA version of the Haslam et al. (1982) 408 MHz map has had both destriping and point source removal algorithms applied to the data, while the 2.3 GHz maps has had no such processing. The free-free model should include significant contributions from many compact HII regions that might have been subtracted from the Haslam map as point sources. To verify that this has no significant impact on our analysis, we compare the profiles of the raw map, the destriped map, and the destriped and point-source subtracted map in Fig. 2. We also compare these locally processed maps to the version available on the LAMBDA⁶ website, which is the version used in our analysis both for this work and in Paper I. The profiles clearly show where a point source was removed, but the effects of the destriping are not visible against the strong emission on the plane. There are only three significant point sources visible (at the Galactic centre, at roughly $\ell \sim 290^\circ = -70^\circ$ and at $\ell \sim 110^\circ$), two of which correspond to features in the MEM free-free estimate. Clearly, the point-source removal is not affecting the free-free subtraction systematically (for example by removing many compact HII regions which would then lead to significant over-subtraction by MEM). What is also clear is that leaving in point sources in the 2.3 GHz map is not likely to have a significant effect on the results when working as we do at large scales.

However, it is worth noting that the source removed at roughly $290^\circ = -70^\circ$ lies on the Carina spiral arm tangent, and as we will show in the results, the model appears to over-predict the synchrotron emission there. This mismatch

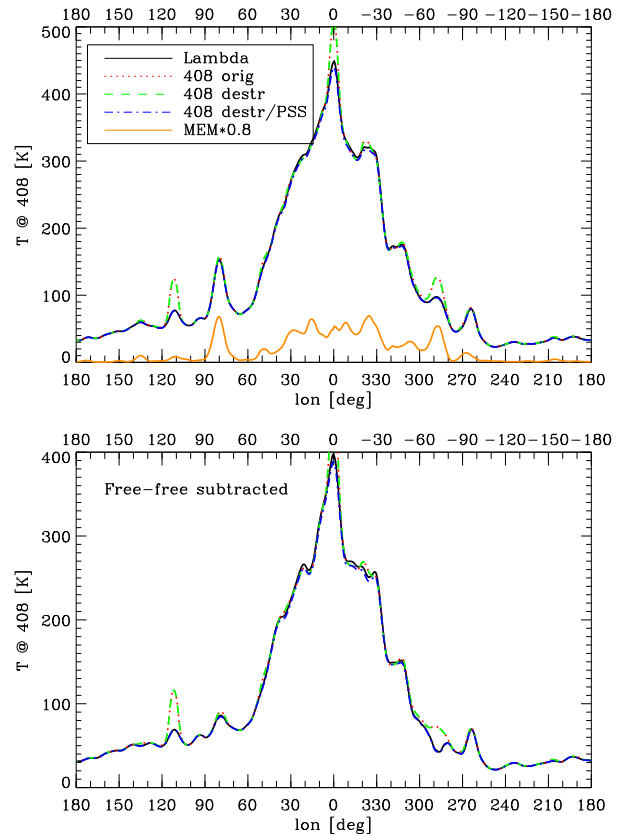


Figure 2. Impact of processing steps on 408 MHz profile. The *top* plot shows the profiles of the LAMBDA map (*black*), the raw 408 MHz map (*red dotted*), the destriped map (*green dashed*), and the destriped and point-source subtracted (PSS) map (*blue dot-dashed*). The *WMAP* MEM free-free profiles is plotted on top in *orange* and subtracted from each of the 408 MHz profiles in the bottom plot.

is perhaps then due simply to the over-subtraction of the free-free from the point-source removed Haslam map.

2.3 Free-free correction

While the synchrotron dominates over the free-free emission over most of the sky, it does not dominate on the Galactic plane itself at any but the lowest of our three synchrotron frequencies. It is because of the free-free that we cannot simply compare the total and polarised emission at the same frequency on the plane: if the frequency is high enough to avoid Faraday effects, then the plane is dominated by free-free emission. Even at the radio frequencies we use, the free-free makes a significant contribution and must be subtracted.

In Paper I, we used the *WMAP* estimate for the free-free emission using the Maximum Entropy Method (MEM) described in Gold et al. (2009) and references therein. One drawback of that analysis is the fact that it attempts to decompose the CMB sky into three components – synchrotron, free-free, and thermal dust emission – when there is clear evidence that a fourth component is significant in all *WMAP* bands but the highest. This fourth component is spatially correlated with the thermal dust emission but has a non-thermal spectrum, and it is widely believed to be due to the

⁶ <http://lambda.gsfc.nasa.gov/>

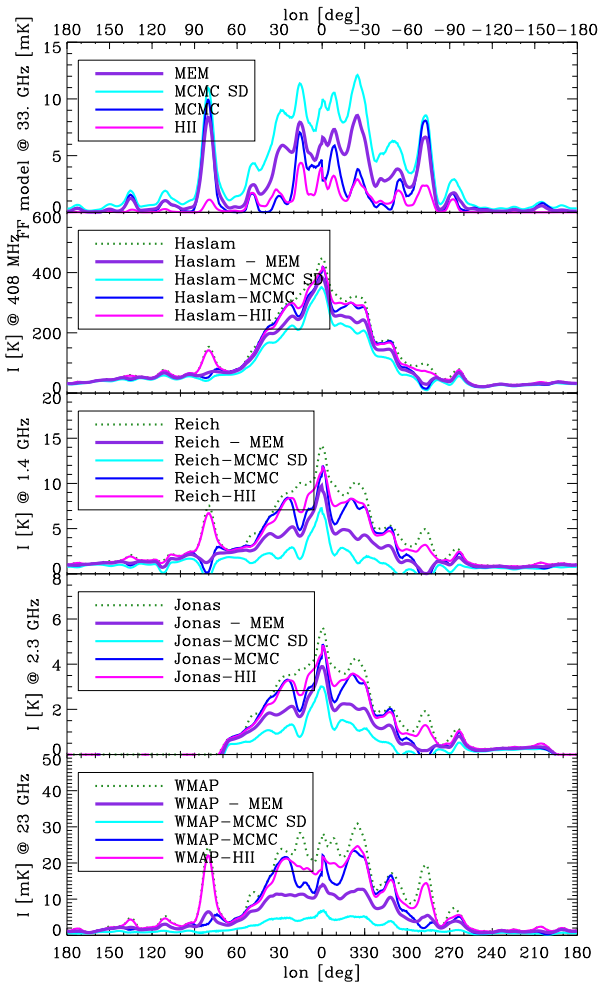


Figure 3. Comparison of free-free emission models. The *WMAP* team produce models using both the MEM and MCMC methods (both with and without spinning dust), while the HII model is based on the Paladini et al. (2003) catalog. See text.

electric dipole emission from spinning dust grains. (See, e.g., Boughn & Pober (2007) or Planck Collaboration (2011) and references therein.) Over the lower *WMAP* frequencies, this emission has a spectrum that roughly follows a power law with an index of $\beta \sim -2.8$ (e.g., Davies et al. 2006). Because this index is closer to the spectrum of synchrotron than to the $\beta = -2.15$ of free-free, one might imagine that the anomalous component would contaminate the MEM synchrotron solution more than the free-free solution. But clearly, the free-free template as well is compromised, and it is difficult to estimate to what degree the MEM free-free solution is an over-prediction.

The more recent *WMAP* seven-year analysis offers an alternative component separation based on pixel-by-pixel MCMC analysis (Gold et al. 2010). This method may also explicitly fit an additional component for the anomalous emission that can vary spectrally from pixel to pixel, while the free-free spectrum is constrained to follow a theoretically motivated power law (Dickinson et al. 2003).

Figure 3 shows the total intensity profiles at each frequency and the free-free correction for different models. In some regions, notably the spiral arm tangent Carina around longitude of $290^\circ = -70^\circ$ and the Cygnus arm around 80° , the MCMC solutions both clearly over-predict the low-frequency free-free and the subtracted profile drops below zero at 1.4 and 2.3 GHz. A vital independent estimate of the free-free emission comes from the study of radio recombination lines (RRLs), where a comparison of ionized hydrogen transition lines to continuum emission allows a measurement of the free-free emission measure. Unlike using H α as a tracer, this measure is not affected by dust absorption and is the only way to measure the free-free on the plane. Alves et al. (2010) have performed such an analysis over a small region of the plane from 36° to 44° longitude. As the most reliable measurement of the free-free emission, it is an interesting region in which to compare the free-free predictions based on the microwave data. The inset of Fig. 4 shows the region analyzed in Alves et al. compared to the models. In that region, the MCMC solution finds no free-free emission in the case without a spinning dust component, while the MCMC result with spinning dust removed significantly over-predicts. The MEM solution, though at lower resolution and far from perfect, more closely reflects the emission measured by the RRL analysis. Alves et al. find that in the region studied, the MEM over-predicts the free-free emission by roughly 20–30 per cent on the plane, presumably due to contamination by the anomalous dust emission.

We have also looked at the catalogue of HII regions by Paladini et al. (2003) to determine the distribution of free-free emission along the plane based on individual compact regions. This does not, of course, take into account the diffuse emission but provides an interesting comparison as a clear minimum amount of emission. Using the catalog of positions and fluxes, Paladini et al. created a smoothed map which we can compare to the diffuse emission data and the other free-free models. This is also shown in Fig. 3.

We conclude that the MCMC free-free predictions appear to be less accurate than the MEM. In some regions, both clearly over-estimate the free-free, while in others they clearly underestimate it. For this reason, we consider the MEM solution to be preferable. As discussed in § 2.1, we studied the offsets of the intermediate frequency datasets as well as the free-free correlation by simply performing linear fits of the 408 MHz profile as a synchrotron template and of the MEM free-free profile. This analysis gives not only a fitted offset but a fitted amplitude of the free-free template compared to the reference dataset. The coefficients are given on the plots in Fig. 5 and show that the free-free fits at an amplitude of lower than 80 per cent of the MEM prediction, consistent with what Alves et al. find. Taking this into account, we lower its amplitude by a conservative 20 per cent when using it to correct each of the total intensity profiles. If we consider this factor of 20 per cent on the free-free correction to be an estimate of a systematic uncertainty in our analysis, then it implies an uncertainty in the spectral index of synchrotron emission from 408 MHz to 2.3 GHz of roughly 0.05.

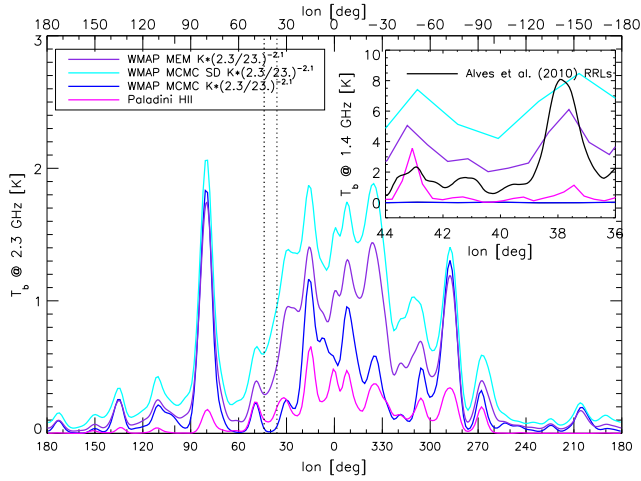


Figure 4. Comparison of the *WMAP* MCMC free-free predictions (with (*cyan*) and without (*blue*) a spinning dust component simultaneously fit) to the MEM solution (*magenta*), both extrapolated to 2.3 GHz, the frequency used in our analysis where the free-free is strongest. Inset is a zoom, this time at 1.4 GHz, of the region shown in Alves et al. (2010) Fig. 10 reproduced here in black. (Note that the inset shows the predictions at their full resolution of 1° , while the main plot is smoothed to 6° .)

3 GALAXY MODELING

Our method follows closely that described in detail in Paper I, so we only summarize briefly here. We use the *HAMMURABI* code (Waelkens et al. 2009) to simulate all the observables (synchrotron total and polarised intensity at each frequency) based on the 3D inputs models for the CREs and the magnetic field. The CRE distribution, both spatial and – newly in this work – spectral, is provided by the *GALPROP* code and Strong et al. (2010), which looks at Fermi γ -ray data. Our magnetic field model is that described in Paper I, though we again allow to vary the B_{RMS} and f_{ord} parameters that determine the strengths of the ordered and isotropic random components. We compare to the datasets described in § 2 using a simple χ^2 to estimate the likelihood of a given parameter set. Again we use the *COSMOMC* code of Lewis & Bridle (2002) as a generic sampler to generate the Markov chains from which we determine the best-fitting model parameters. Where in Paper I we varied B_{RMS} and f_{ord} , in this work we additionally vary the spectral index of the low-energy CRE injection spectrum.

In the following sections, we describe these changes in more detail.

Note that since we do not vary the parameters of the coherent magnetic field, nor the thermal electron density, in this work we do not make further use of the rotation measure data or model prediction. (The polarisation frequency we use is at high enough frequency that, though the RM is properly computed and applied in *HAMMURABI*, it is negligible.) It is important, however, to remember the constraint that these data place on the coherent field strength as demonstrated in Paper I. These data and model remain important to visualizing the morphology of the field in the plane, so we continue to plot them with our synchrotron data.

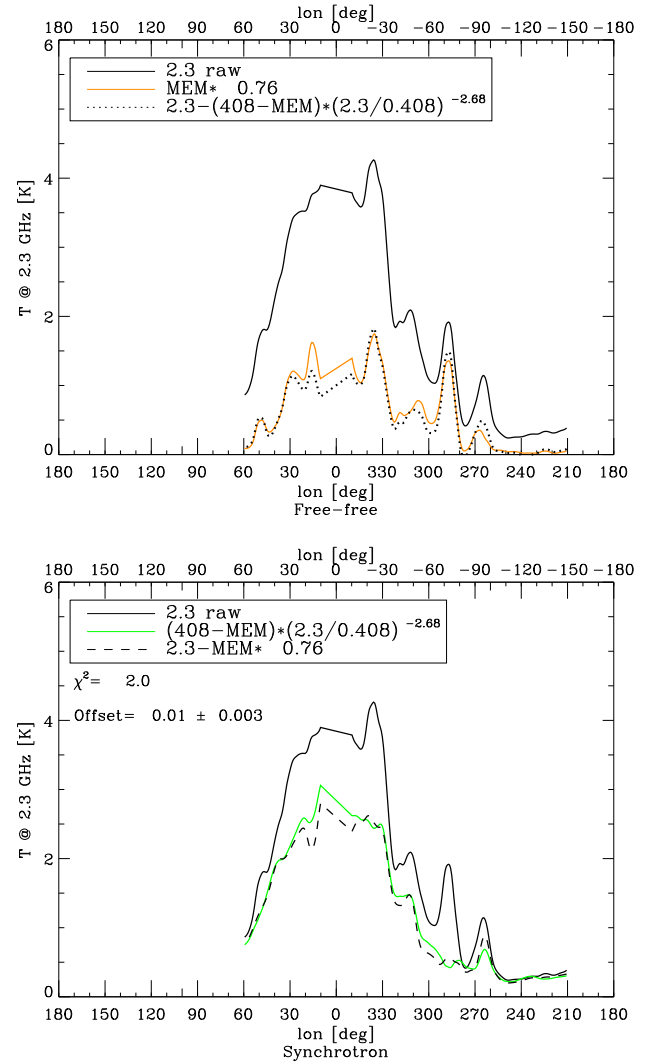


Figure 5. Comparison of 2.3 GHz survey with 408 MHz survey and the MEM free-free model on the plane. In both plots, the *solid black* curve shows the full 2.3 GHz survey profile along the plane. We then fit both synchrotron and free-free templates and compare the residuals to the scaled templates. See text. *On the top* are shown fitted the MEM free-free solution (*orange*) and profile after the fitted 408 MHz synchrotron profile is subtracted (*dotted black*). *On the bottom*, we see the synchrotron residuals (*dashed black*) after we subtract the fitted MEM compared to the fitted 408 MHz profile (*green*). The scale factors of the fits are given in the legends, as a spectral index in the case of synchrotron, while the offset is printed below the legend.

3.1 Cosmic-ray electrons: GALPROP

We use the *GALPROP* code to propagate primary electrons and secondary positrons and electrons and thereby to model the resulting distribution of Galactic cosmic ray electrons and positrons. The inputs are models of particle injection spectra (primary electrons and protons), the smooth spatial distribution of sources, the interstellar radiation environment, diffusion processes, and synchrotron losses based on a model magnetic field. The secondary lepton source function

Parameter	z04LMS	z04LMPDS
D0 _{xx}	5.8×10^{28}	3.4×10^{28}
D _{g_0}	0.33	0
D _{g_1}	0.33	0.5
v _{Alfven}	30.	-
electron _{g_1}	2.4	2.3
electron _{norm_flux}	0.32×10^{-9}	0.32×10^{-9}

Table 1. Comparison of two GALPROP models used (i.e. GALDEF contents). The z04LMS model includes re-acceleration, while z04LMPDS is pure diffusion. Only the physical parameters are given; other GALDEF differences include the spectral energy resolution, as the model with re-acceleration is more sensitive to the resolution at low energies, while without re-acceleration, the propagation can be sped up.

is obtained from the CR proton distribution.⁷ Our baseline is the “z04LMPDS” model from Strong et al. (2010) with a few modifications. We also test the “z04LMS” from the same paper, the main difference being the fact that the latter includes the effects of re-acceleration. See § 4.4.

We have lowered the simulation spectral range (here 0.2 to 1000 GeV) and resolution (sampling as $E_i = E_0 2^i$) as much as possible to speed up the propagation, testing with each change that the results for our relevant observables remain unchanged, and replaced the GALPROP magnetic field model with our own. There are several things to note about the magnetic field in GALPROP. Though our field model has a trivial constant vertical structure, and though GALPROP will use the field up to 4 kpc off the plane in the propagation, we find that the resulting CRE distribution on the plane is not affected by this inaccuracy. Secondly, note that the small-scale B-field variations have negligible effect on the electron spectrum since electrons sample a very large region during propagation in the galaxy. Only the strength of the total field is relevant for electron energy losses. Furthermore, note that in GALPROP there is no explicit connection between the B-field and the cosmic-ray diffusion coefficient, since the latter is derived observationally from nuclei secondary-to-primary ratios.

We can then explore the low-energy end of the cosmic ray spectrum by varying the spectral index of the injected electron spectrum below 4 GeV. This energy range is so far ill-constrained, as solar modulation affects local measurements of CRE densities. (The “z04LMPDS” default for this parameter was -1.6 .)

See Table 1 for a list of the parameters that differ between the two models. An example and comparison with data is shown in Fig. 6.

3.2 Integration

In Paper I, we computed the total synchrotron emission along the line of sight by assuming a power law distribu-

⁷ For speed, we do not include Helium in the propagation, which does produce additional secondary leptons. We determined that the contribution is too small to make a significant difference to the resulting synchrotron.

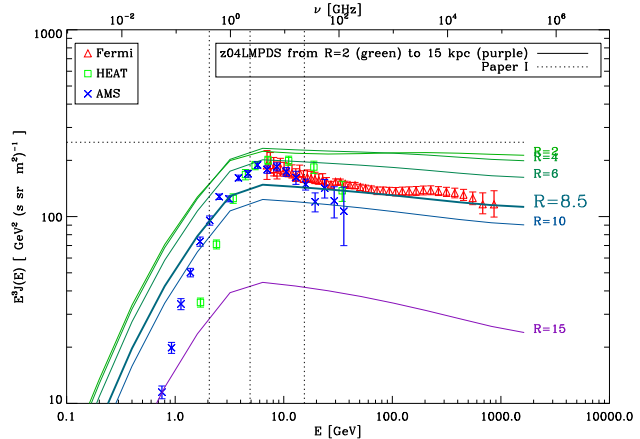


Figure 6. Comparison of example GALPROP cosmic ray spectra at different galacto-centric radii to the simple power law spectrum as used in Paper I. Vertical dotted lines mark the frequencies 408 MHz, 2.3 GHz, and 23 GHz. Over-plotted are data from Fermi (Ackermann et al. 2010), HEAT (DuVernois et al. 2001), and AMS (Aguilar & et al. 2002) using the database of Strong & Moskalenko (2009). The top axis indicates approximately the effective synchrotron frequency corresponding to the electron energy on the lower axis, assuming a field strength of $6 \mu\text{G}$; see text and Eq. 3. Note that the predicted interstellar spectra are not expected to match the data below 10 to 20 GeV due to solar modulation; see § 4.5.

tion of CREs:

$$I_{\text{sync}}(\nu, p) \propto \int_{\text{LOS}} dr J_{\text{CRE}}(\mathbf{r}) B_{\perp}(\mathbf{r})^{\frac{p+1}{2}} \quad (1)$$

where I is the specific intensity and $J_{\text{CRE}}(\mathbf{x})$ is the density of cosmic ray electrons (CREs) described explicitly in § 3.1. The total intensity, or Stokes I, in a given observing beam is then $I = \int I d\Omega$. We assumed, as is commonly done, $p = 3$, where the CRE distribution is $N(\gamma)d\gamma \propto \gamma^{-p}d\gamma$. This then implies that $I(\nu_1)/I(\nu_2) = (\nu_1/\nu_2)^{-3}$.

But since we are now using the full spectral information given by GALPROP, we must perform the full integration over electron energies γ . At each position, the total synchrotron power is:

$$P_{\text{tot}}(\mathbf{r}, \omega) \propto \int dx J_{\text{CRE}}(\mathbf{r}, \gamma) B_{\perp}(\mathbf{r}) F(x) \quad (2)$$

where $x \equiv \frac{\omega}{\omega_c}$ and $\omega_c \equiv \frac{3\gamma^2 B_{\perp}}{2mc}$. The function $F(x)$ is an integral over modified Bessel functions. (In our modified HAMMURABI code, we use the GNU Scientific Library⁸ to compute these.) See, e.g., Rybicki & Lightman (1979) for details and for the expressions for determining the Stokes parameters; the above expression is simply to clarify the dependencies.

3.3 MCMC

The likelihood exploration is performed as in Paper I with the addition of a third varied parameter, GALPROP’s `electrong_0` that defines the spectral index of the CRE

⁸ <http://www.gnu.org/software/gsl/>

injection spectrum below 4 GeV. (This is related to the spectral index p in Eq. 1 but not the same; the injection spectrum described by `electron_g_0` will be subsequently modified by the various mechanisms in the propagation.) This does not fundamentally change the process but simply implies that we need more samples to obtain convergence in the likelihood distribution. Because of the further added computational difficulty of running a GALPROP propagation for each sample, the computation of each sample is slowed by a factor of three. The third parameter is not strongly correlated with the others, so the likelihood distributions remain roughly independent and Gaussian.

4 RESULTS

4.1 Observables

Figure 7 shows the results of fitting three parameters to the three synchrotron profiles (total intensity at 408 MHz and 2.3 GHz, polarised intensity at 23 GHz) using the plain diffusion z04LMPDS CR model. Two parameters, B_{RMS} and f_{ord} , control the ratios of the three magnetic field components (where the coherent field is fixed at the values found in Paper I using the RM data) along with the `electron_g_0` parameter of GALPROP, which is the spectral index of the electron injection spectrum below the first break, i.e. for energies less than 4 GeV.

The magnetic field parameters differ from our results in Paper I due to the fact that the CRE spectrum is different. Figure 7 shows the new fit results, giving a low-energy spectral index of -1.34 ± 0.12 , which is harder than the GALPROP default of -1.6 usually used (e.g., Trotta et al. 2011; Ackermann et al. 2010).

The fit residuals are shown in Fig. 8. The model corresponding to the best-fitting parameters from the MCMC analysis is shown in red compared to the data in green. The dotted red line represents the ‘galactic variance’, i.e. the amount any individual galaxy realization can be expected to vary from the average profile due to its turbulent component. In general, the profiles match well, but there are deviations where individual arm tangents are not well modeled (Sagittarius and Carina) or where the data contain unrelated objects such as supernova remnants. Though its centre is off the plane, Vela is large enough and bright enough that it is clearly visible in the smoothed plane profiles of both 408 MHz and 2.3 GHz. The CasA supernova remnant is also visible around 112° longitude in the 408 MHz total intensity profile.

As noted in § 2.2, the point source removal processing on the Haslam map appears to have removed something in the direction of the Carina arm tangent. If this was a compact HII region that is still contributing to the free-free correction, then the data used will have been over-subtracted there. This could explain the mismatch between the model and data for this arm.

It is also interesting to note that the Sagittarius arm does not fit well, as the model significantly over-predicts the emission along that tangent. The Cordes & Lazio (2002) (a.k.a. NE2001) model for the thermal electron distribution uses a similar spiral arm model, one of which, the Sagittarius arm, appears to have a missing segment in precisely the

direction where our model over-predicts. While synchrotron is not dependent on the distribution of thermal electrons, the rough agreement elsewhere between the synchrotron arm tangents and the known spiral arms included in the NE2001 model does imply that the distribution of the various components of the magneto-ionic medium are not independent. It does indeed appear that either the total magnetic field or the distribution of cosmic rays also fails to follow the modeled Sagittarius arm inward of the Sun’s position.

Furthermore, as discussed above, there are new RM data by Van Eck et al. (2011) that shed light on this issue. Van Eck et al. do not attempt to fit a coherent spiral arm model similar to ours but rather take a simpler approach to determine the field direction in each of a set of segments. These segments are delineated by a spiral in the inner galaxy quadrant defined largely by negative longitudes and by simple annuli in the rest of the inner galaxy. With this prescription, they can create a model to match the peaks and troughs in all the RM data, but this model obviously has far more parameters than our global model. It is interesting to note, however, that the van Eck et al. data are inconsistent with our model in the newly covered region from roughly 20° to 60° longitude. The data show a peak of roughly the same amplitude, implying the same coherent field strength, but shifted outward. Clearly the coherent field does not follow our model of the Sagittarius-Carina arm from the first to third quadrants. Note that the NE2001 model also predicts a ‘bite’ taken out of its otherwise similar spiral arm model in the direction of Sagittarius. To construct a model consistent with all observations is now increasingly challenging, which is an improvement over the previous situation of having too many possible models. It is also beyond the scope of this paper, though we will address the issue in future work that will also make use of Planck data. Note that this inconsistency is in the geometry and not the strength of the magnetic field components and therefore does not impact the current scientific results based on the synchrotron spectrum.

We note that the best-fitting polarisation profile appears systematically slightly higher than the data. (The fact that the χ^2 remains near one is due to the large and forgiving variance from the turbulent field component.) It is overly simplistic to say that we can perfectly fit our three synchrotron frequencies by varying three parameters: B_{RMS} , f_{ord} , and `electron_g_0`. The total magnetic field strength does have an impact on the CRE spectrum at energies above a few GeV, where the 23 GHz synchrotron will be affected. To correct this bias, one might lower f_{ord} , but this would lower the total magnetic field strength, reduce the CRE synchrotron losses, harden the CRE spectrum above a few GeV, and thereby harden the synchrotron as well. Therefore we cannot correct the bias with only our three parameters. The implication is that the GALPROP parameter `electron_g_1` determining the injection spectral index between 4 GeV and 1 TeV should be steeper than the -2.25 found in Strong et al. (2010) with a different magnetic field model. If we had unlimited computational resources, we should simultaneously explore more of the GALPROP parameters and include Fermi CRE and γ -ray data, but this is not currently feasible.

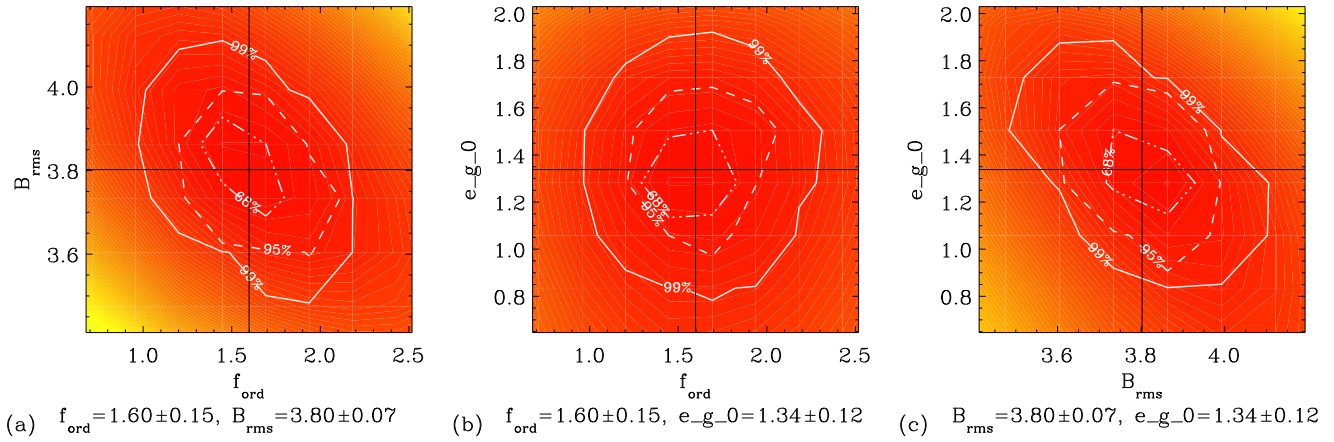


Figure 7. Results of MCMC chain. The color gives an indication of the sample density, while the contours give the 1, 2, and 3 σ confidence regions. The cross-hairs show the mean values, also printed below each set with their uncertainties. For comparison, the Paper I results of the two-parameter fit using only 408 MHz and 23 GHz were: $f_{\text{ord}} = 1.5 \pm 0.16$ and $B_{\text{RMS}} = 2.1 \pm 0.04$. The profiles and residuals are shown in Fig. 8.

4.2 Synchrotron spectral index

Fig. 9 shows the synchrotron spectral index between each pair of frequencies as a function of longitude. The implied synchrotron spectral index from 408 MHz and 2.3 GHz is roughly $-2.8 < \beta < -2.74$, and that between 2.3 GHz and 23. GHz is $-2.91 < \beta < -2.98$ depending on the longitude. Previous synchrotron spectral index analyses that don't explicitly exclude the plane (Reich & Reich 1988; Davies et al. 1996; Giardino et al. 2002; Platania et al. 2003) tend not to discuss it in detail either because of the uncertainties in the free-free contamination or simply because they are primarily interested in high latitudes. Most do conclude with a low-frequency spectral index of roughly -2.8 and a high frequency index of roughly -3 .

Recall that our method computes the synchrotron emissivity at each frequency and at each Galactic position independently based on the input spatial and spectral distribution of CRE injection sources, the interstellar radiation field (ISRF), and of course the Galactic magnetic field. Because all of the other components are azimuthally symmetric about the Galactic centre, the structure seen in Fig. 9 is a result of the changing magnetic field strength when looking in different directions. This affects the synchrotron spectral index as can be seen both via Eq. 2 as well as more simply via an approximation of the effective synchrotron frequency for an electron of a given energy:

$$\nu_{\text{eff}}[\text{MHz}] = 16B_{\perp}[\mu\text{G}]E^2[\text{GeV}^2] \quad (3)$$

from Webber et al. (1980). The steep spectral break at 4 GeV means that a change in the field strength changes the region of the electron index that the radio synchrotron frequencies are effectively sampling, which in turn can have a large effect on the predicted synchrotron spectral index.

The structure of each of the synchrotron index profiles shows the hardest emission toward the anti-centre and the softest emission toward $\ell \sim 300^\circ = -60^\circ$. The Galactic centre region $-60^\circ \lesssim \ell \lesssim 50^\circ$ is bracketed asymmetrically by softer-spectrum dips on either side, which hints at the source being the spiral magnetic field morphology. Such an asymmetry is expected for a modulation related to

the strong Scutum-Crux and Perseus arms. The latter, passing behind the Solar position would explain the anti-centre hardening. (Recall from Paper I that the results indicated that the Sagittarius-Carina arm is very weak in terms of the magnetic field strength, and the Norma arm not well constrained.) Note that a similar figure produced using a simple exponential disc magnetic field model, e.g. the GALPROP default, shows no such structure; instead there is only a very slight hardening toward the Galactic centre as one would expect.

The measured spectral index between the two total intensity frequencies is also shown in Fig. 9 as the black dashed line. Its variation along the plane (due to the turbulent variations in the magnetic field) is larger than the predicted *average* features of Fig. 9, so it is unlikely we can ever confirm such structures. We can also see that there is again a small bias in that spectral index; the best-fitting model returns an average spectral index between 0.408 and 2.3 GHz of roughly -2.75 , while the data show a slightly harder average of around -2.7 . As discussed above, this is due to the fact that the three parameters varied do not have complete freedom to fit the data perfectly due to the complicated inter-feraction of the magnetic field strength and the cosmic ray distribution in determining the resulting synchrotron. If we had the computational resources to vary more of the GALPROP parameters (and necessarily include the Fermi electron and γ -ray data which also constrain them), we would expect a model with a slightly harder low-frequency spectrum and a slightly steeper high-frequency spectrum. (This can just be seen by eye in Fig. 8 as a slight positive bias in the model at 408 MHz.) Though we have varied the low-energy electron spectrum, we have not varied the high-energy end, which is the source of the bias.

4.3 CRE spectrum

The resulting CRE spectrum is shown in Fig. 10. At higher energies, above roughly 20 GeV, it is consistent with the Fermi data. Below these energies, the local measurements are not directly comparable to the model due to solar mod-

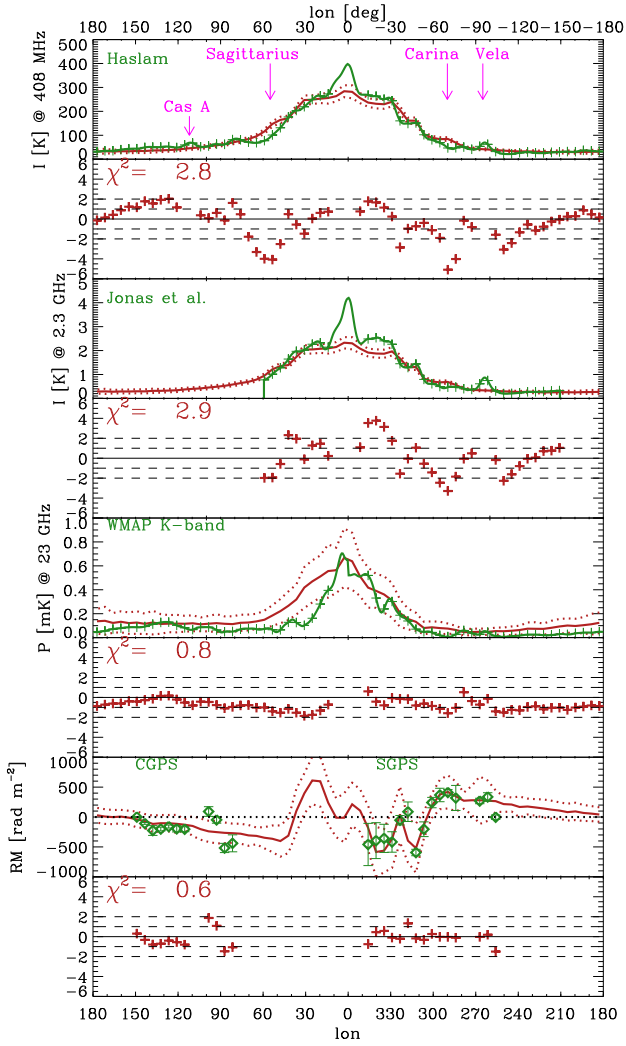


Figure 8. Best-fitting model (*red solid*) with its expected variations (*red dotted*) compared to the data (*green*) for each observable. The computed χ^2 excludes problem regions like the Galactic centre and the Cas A and Vela supernova remnants.

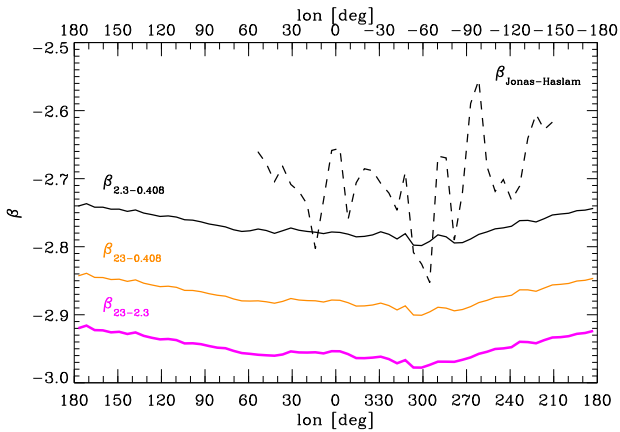


Figure 9. The best-fitting model’s synchrotron spectral indices between each of the set of synchrotron frequencies. For comparison, the spectral index from Haslam 408 MHz to Jonas et al. 2.3 GHz is over-plotted. See text.

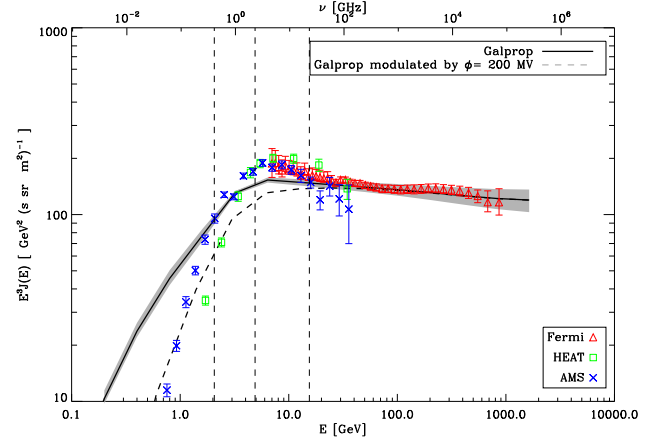


Figure 10. Best-fitting CRE spectral prediction for the Solar neighborhood (*solid black*) compared to Fermi, HEAT, and AMS data. The grey shading indicates the region of uncertainty: at low energies, bounded by the 1σ uncertainty in the electron injection spectral index, and at high energies, due to the variance in the local magnetic field. The *dashed black* line shows an attempt to modulate this spectrum with the Gleeson & Axford (1968) prescription using $\phi = 200$ MV, which clearly does not work at all energies. Lastly, note that this spectrum is *not* a fit to the Fermi CRE data but rather uses parameters constrained with Fermi γ -ray data and yet shows good consistency at high energies.

ulation. The best-fitting value of the low-energy electron injection spectrum gives $J(E) \propto E^{-1.34}$, which is slightly harder than the previous GALPROP default value of -1.6 . That figure also shows in shaded grey the uncertainty in the low-energy end of the spectrum due to the error bar on that index as estimated by our MCMC chains. The fact that this uncertainty appears so small is due to the sensitive dependence of the synchrotron amplitudes and our fairly precise fitting on the plane. The shaded grey at high energies shows the uncertainty due to a different source. The parameters are fit by comparing a synchrotron profile along the plane, which averages through the galaxy, to many independent simulations of a magnetic field that includes a stochastic component. What we are plotting in this figure is the predicted cosmic ray spectrum at the solar position compared to locally measured CREs. But that local measurement is affected by any fluctuation in the local magnetic field. To account for this uncertainty, we compute a mean spectrum at the solar radius and the corresponding variance to give an idea of how much the high-energy end of the local spectrum can vary due to localized magnetic field fluctuations. (This affects only the higher energy end of the spectrum, because it is at high energies that synchrotron energy losses are most severe and therefore most affected by local fluctuations.)

The uncertainty in the CRE injection spectral index returned by the MCMC analysis is the statistical uncertainty due to the “galactic variance” from the turbulent field component. There remains a systematic uncertainty due to the free-free correction discussed in § 2.3. This effect, however, is smaller than the galactic variance, as it implies a possible error on the synchrotron index of only 0.05.

4.4 Re-acceleration

The “z04LMS” model from Strong et al. (2010) includes diffusive re-acceleration. The addition of this process to the propagation helps to reproduce an observed peak in the secondary to primary particle ratio, though the evidence for the process as implemented in z04LMS is not unambiguous; see Strong et al. 2007. The effect of this process on the total interstellar CRE spectrum is an additional bump around a few GeV. This region of the spectrum is responsible for synchrotron bands at 408 MHz and 2.3 GHz.

Using the parameters of the “z04LMS” model and varying only the spectral index of the injection spectrum below 4 GeV, we are unable to find a fit consistent with the synchrotron data. The MCMC tend toward `electron_g_0` of zero, which is simply because that is the only way to counter the effect of the re-acceleration bump and leave a CRE spectrum in the few GeV range that is consistent with the radio synchrotron data. Either the re-acceleration is not correct, or we must vary other parameters such as those defining the diffusion, which would then risk a result inconsistent with the γ -ray and other data that model was made to fit.

4.5 Solar modulation

Though various satellites have directly measured the flux of cosmic ray electrons near the Earth, these measurements do not reflect the average distribution of particles in the ISM. The reason is the interaction of the CREs with the solar wind. In essence, there are magnetic irregularities carried with the solar wind that scatter lower energy CREs. Not only is it difficult to quantify the modulation of the CRE spectrum, but the modulation is time-varying. Gleeson & Axford (1968) give a simple prescription based on a single parameter for modulating a CRE spectrum using the force field approximation to account for this solar system effect. Though a simple approximation, this prescription remains in use (Ackermann et al. 2010; Trotta et al. 2011) for lack of a significantly better alternative. Using this method, DuVernois et al. (2001) estimated 755 MV for 1994 and 670 MV for 1995, the relevant time periods for the HEAT observations, while Aguilar & et al. (2002) estimate 650 ± 40 MV for their 1998 observations. These figures, however, generally depend on an assumed interstellar CRE spectrum with a steeper low-energy CRE injection spectral index (-2.1), which is now ruled out by the synchrotron data.

The only way to study the CRE spectrum at lower energies, then, is to use a tracer such as synchrotron emission or inverse-Compton γ -rays. Unfortunately, on the Galactic plane, the γ -ray spectrum is dominated by the gas component rather than the inverse Compton component (and that is in turn dominated by higher energy CREs or nuclei) so that the γ -ray data cannot help us much with the low-energy CRE spectrum. It is certainly possible to produce plots of modulated theoretical CRE spectra matching even the low-E data such as Fig. 22 of Ackermann et al. (2010). However, as discussed in § 4.4, this is due to a combination of adding an uncertain re-acceleration process and using a simplistic solar modulation prescription. It is unclear that we are learning anything meaningful about either process.

Examining the synchrotron emission is therefore a more reliable way to explore the low-energy CRE spectrum. With

enough frequencies, we can overcome degeneracies with the magnetic field parameters and obtain a more accurate determination of the CRE spectral index below a few GeV. It would be easier if we could use even lower-frequency synchrotron data, but on the plane, emission much lower than 408 MHz is going to be absorbed by ionized gas.

It is therefore interesting to note that in Fig. 10, we see that for our best fit parameters, the simple Gleeson & Axford solar modulation prescription does not match the local observations at low energies. For lower values of Φ , the spectrum at the lowest energies would be too high, while at the value of 200 MV as shown, the predicted spectrum is already too low at intermediate energies of roughly 3 to 20 GeV. To match all of the data without re-acceleration would therefore require a different solar modulation model. Likely this is an unsurprising indication that a more sophisticated treatment of the modulation is needed or that the cosmic ray propagation needs to be modified in the few GeV regime.

The spectrum in Fig. 10 also shows that the local measurements are in excess of the the interstellar prediction around the region of the break at 4 GeV. Even a more accurate solar modulation model is unlikely to fix this problem.

5 CONCLUSIONS

We have used a self-consistent method of modeling both the Galactic magnetic field and the cosmic ray electron spectrum in the Galactic plane and used comparisons with synchrotron data to constrain physical parameters of the model. The particular advantage of this analysis over previous analyses is our ability to constrain simultaneously the CREs and magnetic field in the plane while taking into account the field’s effect on the CRE propagation. Using multiple synchrotron frequencies and the combination of total intensity and polarised intensity, we can constrain not only the magnetic field parameters as in Paper I but also begin to provide among the first constraints on the low-energy CRE spectrum. This regime of the CRE distribution is not accessible via either inverse-Compton γ -ray production or through direct measurement, since the locally measured distribution is affected by solar modulation.

We find that the magnetic field parameters measured in Paper I must be modified slightly when a realistic CRE spectrum is taken into account. In particular, the random component is even larger compared to the coherent component, with $B_{\text{RMS}} = 3.8$ compared to 2.1 in our previous work (see Jaffe et al. 2010 for the field parametrization). The large change illustrates both the significance of dropping the assumption of a single CRE spectral index from below a GeV to 10^2 GeV, which was not realistic, and the fact that our fitting returns a much harder low-energy spectral index requiring a large magnetic field change to compensate. This does not change the main point of that first paper, which was to demonstrate the importance of the ordered component of the magnetic field, since the ratio of the ordered component to the isotropic random component remains roughly unchanged. The implication is an even stronger turbulent Galactic magnetic field; the isotropic component has a peak RMS of nearly 8 μG along the arm ridges, while the total

field strength on the ridge is then as much as 15 μG compared to roughly 5 μG in the inter-arm regions.

The fitting of the low-energy cosmic ray injection spectrum gives us a slightly harder spectrum of than is generally assumed. The GALPROP parameter `electron_g_0` representing the spectral index of the injection spectrum below 4 GeV, is determined to be 1.34 ± 0.12 , though the oft-used value of 1.6 is not strongly ruled out. Our more robust measure of the index implies a somewhat harder injection spectrum and confirms the strong break at a few GeV between the low energy regime with an index of -1.3 and the higher energy range, with an index of roughly -2.3 . We find the re-acceleration model to be incompatible with the low-frequency synchrotron data for any value of the CRE spectral index. Lastly, we find that the shape of the predicted CRE spectrum combined with the force field approximation to the solar modulation is not able to reproduce the local measurements of the CRE density. More work is needed to find a model consistent with all the available datasets.

ACKNOWLEDGMENTS

We gratefully acknowledge useful discussions with C. Evoli, C. Dickinson, R. Davies, and W. Reich. We thank J. Jonas for the 2326 MHz data as well as M. Alves for the RRL data plotted in Fig. 4 and R. Paladini for the HII data. We acknowledge use of the HEALPix software (Górski et al. 2005) for some of the results in this work. We acknowledge the use of the Legacy Archive for Microwave Background Data Analysis (LAMBDA). Support for LAMBDA is provided by the NASA Office of Space Science.

REFERENCES

- Abdo A., et al., 2009, *PhysRevLett*, 103, 251101
 Ackermann M., et al. 2010, *PhysRevD*, 82, 092004
 Aguilar et al. 2002, *PhysReports*, 366, 331
 Alves M. I. R., Davies R. D., Dickinson C., Davis R. J., Auld R. R., Calabretta M., Staveley-Smith L., 2010, *MNRAS*, 405, 1654
 Bennett C. L. et al., 2003, *ApJS*, 148, 97
 Boughn S. P., Pober J. C., 2007, *ApJ*, 661, 938
 Brown J. C., Haverkorn M., Gaensler B. M., Taylor A. R., Bizunok N. S., McClure-Griffiths N. M., Dickey J. M., Green A. J., 2007, *ApJ*, 663, 258
 Brown J. C., Taylor A. R., Jackel B. J., 2003, *ApJS*, 145, 213
 Cordes J. M., Lazio T. J. W., 2002, preprint (astro-ph/0207156)
 Davies R. D., Dickinson C., Banday A. J., Jaffe T. R., Górski K. M., Davis R. J., 2006, *MNRAS*, 370, 1125
 Davies R. D., Watson R. A., Gutierrez C. M., 1996, *MNRAS*, 278, 925
 Dickinson C., Davies R. D., Davis R. J., 2003, *MNRAS*, 341, 369
 Duncan A. R., Haynes R. F., Jones K. L., Stewart R. T., 1997, *MNRAS*, 291, 279
 DuVernois M. A. et al., 2001, *ApJ*, 559, 296
 Giardino G., Banday A. J., Górski K. M., Bennett K., Jonas J. L., Tauber J., 2002, *A&A*, 387, 82
 Gleeson L. J., Axford W. I., 1968, *ApJ*, 154, 1011
 Gold B. et al., 2009, *ApJS*, 180, 265
 Gold B. et al., 2011, *ApJS*, 192, 15
 Górski K. M., Hivon E., Banday A. J., Wandelt B. D., Hansen F. K., Reinecke M., Bartelmann M., 2005, *ApJ*, 622, 759
 Guzmán A. E., May J., Alvarez H., Maeda K., 2011, *A&A*, 525, 138
 Haslam C. G. T., Stoffel H., Salter C. J., Wilson W. E., 1982, *A&AS*, 47, 1
 Jaffe T. R., Leahy J. P., Banday A. J., Leach S. M., Lowe S. R., Wilkinson A., 2010, *MNRAS*, 401, 1013
 Jarosik N. et al., 2011, *ApJS*, 192, 14
 Jonas J. L., Baart E. E., Nicolson G. D., 1998, *MNRAS*, 297, 977
 Lawson K. D., Mayer C. J., Osborne J. L., Parkinson M. L., 1987, *MNRAS*, 225, 307
 Lewis A., Bridle S., 2002, *PRD*, 66, 103511
 Paladini R., Burigana C., Davies R. D., Maino D., Bersanelli M., Cappellini B., Platania P., Smoot G., 2003, *A&A*, 397, 213
 Planck Collaboration, 2011, preprint (astro-ph/1101.2031)
 Platania P., Burigana C., Maino D., Caserini E., Bersanelli M., Cappellini B., Mennella A., 2003, *A&A*, 410, 847
 Reich P., Reich W., 1986, *A&AS*, 63, 205
 Reich P., Reich W., 1988, *A&A*, 196, 211
 Reich W., 1982, *A&AS*, 48, 219
 Rybicki G. B., Lightman A. P., 1979, *Radiative Processes in Astrophysics*, John Wiley & Sons, New York
 Strong A., Porter T., Digel S., Jóhannesson G., Martin P., Moskalenko I., Murphy E., Orlando E., 2010, *ApJL*, 722, L58
 Strong A. W., Moskalenko I. V., 2009, *Proceedings of the 31st ICRC, Lodz, Poland, 2009*, preprint (astro-ph/0907.0565)
 Strong A. W., Moskalenko I. V., Ptuskin V. S., 2007, *Annual Review of Nuclear and Particle Science*, 57, 285
 Taylor A. R., Stil J. M., Sunstrum C., 2009, *ApJ*, 702, 1230
 Trotta R., Jóhannesson G., Moskalenko I. V., Porter T. A., de Austri R. R., Strong A. W., 2011, *ApJ*, 729, 106
 Uyaniker B., Landecker T. L., Gray A. D., Kothes R., 2003, *ApJ*, 585, 785
 Van Eck C., Brown J., Stil J., Rae K., Mao S., Gaensler B., Shukurov A., Taylor A., Haverkorn M., Kronberg P., McClure-Griffiths N., 2011, *ApJ*, 728, 97
 Waelkens A., Jaffe T., Reinecke M., Kitaura F. S., Enßlin T. A., 2009, *A&A*, 495, 697
 Webber W. R., Simpson G. A., Cane H. V., 1980, *ApJ*, 236, 448

This paper has been typeset from a \TeX / \LaTeX file prepared by the author.